

Contents lists available at ScienceDirect

Talanta

journal homepage: www.elsevier.com/locate/talanta





Comprehensive analysis of alkenones by reversed-phase HPLC-MS with unprecedented selectivity, linearity and sensitivity

Sian Liao ^a, Xiao-Lei Liu ^b, Katherine E. Manz ^c, Kurt D. Pennell ^c, Joseph Novak ^d, Ewerton Santos ^e, Yongsong Huang ^{e,*}

- ^a Department of Chemistry, Brown University, 324 Brook Street, Providence, RI, 02912, USA
- ^b School of Geosciences, University of Oklahoma, 100 E. Boyd Street, Norman, OK, 73019, USA
- ^c School of Engineering, Brown University, 345 Brook Street, Providence, RI, 02912, USA
- ^d Ocean Sciences Department, University of California, Santa Cruz, CA, 95064, USA
- e Department of Earth, Environmental and Planetary Sciences, Brown University, 324 Brook Street, Providence, RI, 02912, USA

ARTICLE INFO

Handling Editor: Ian D McKelvie

Keywords: Alkenones Reversed-phase HPLC APCI ESI Orbitrap

ABSTRACT

Alkenones are among the most widely used paleotemperature biomarkers. Traditionally, alkenones are analyzed using gas chromatography-flame ionization detector (GC-FID), or GC-chemical ionization-mass spectrometry (GC-CI-MS). However, these methods encounter considerable challenges for samples that exhibit matrix interference or low concentrations, with GC-FID requiring tedious sample preparations and GC-CI-MS suffering from nonlinear response and a narrow linear dynamic range. Here we demonstrate that reversed-phase high pressure liquid chromatography-mass spectrometry (HPLC-MS) methods provide excellent resolution, selectivity, linearity and sensitivity for alkenones in complex matrices. We systematically compared the advantages and limitations of three mass detectors (quadrupole, Orbitrap, and quadrupole-time of flight) and two ionization modes (electrospray ionization (ESI) and atmospheric pressure chemical ionization (APCI)) for alkenone analyses. We demonstrate that ESI performs better than APCI as response factors of various unsaturated alkenones are similar. Among the three mass analyzers tested, orbitrap MS provided the lowest limit of detection (0.4, 3.8 and 8.6 pg injected masses for Orbitrap, qTOF and single quadrupole MS, respectively) and the widest linear dynamic range (600, 20 and 30 folds for Orbitrap, gTOF and single quadrupole MS, respectively). Single quadrupole MS operated in ESI mode provides accurate quantification of proxy measurements over a wide range of injection masses, and with its modest instrument cost, represents an ideal method for routine applications. Analysis of global core-top sediment samples confirmed the efficacy of HPLC-MS methods for the detection and quantification of paleotemperature proxies based on alkenones and their superiority over GC-based methods. The analytical method demonstrated in this study should also allow highly sensitive analyses of diverse aliphatic ketones in complex matrices.

1. Introduction

Long-chain alkenones have been widely and successfully applied in paleoceanography and paleoclimatology for over 40 years [1–3]. Traditionally, alkenones are analyzed using GC-FID, which is generally sufficient for measuring the common paleothermometer $U_{37}^{K'}$. $U_{37}^{K'}$ represents the relative abundances of $C_{37:2}$ and $C_{37:3}$ alkenones ($U_{37}^{K'} = C_{37:2}/(C_{37:2} + C_{37:3})$, where $C_{37:2}$ and $C_{37:3}$ represent C_{37} straight chain methyl ketones with 2 and 3 double bonds, respectively). This index displays strong linear relationship with sea surface [4] or aquatic

environmental temperatures [5–8]. However, GC-FID encounters considerable difficulties in analyzing alkenones that are of low concentration and contain large amounts of coelutions [8–11]. Saponification can remove esters [12], but it extends sample workup time, lowers alkenone recovery, and has been reported to bias the reconstructed sea surface temperatures (SST) by up to 2.2 °C in a global lab survey [13]. Steryl ethers, which are common in marine sediments overlain by cool surface waters (such as high latitude or upwelling regions) and sites with significant continental inputs, require even greater effort (e.g., using preparative high pressure liquid chromatography (HPLC) and silver

E-mail address: yongsong_huang@brown.edu (Y. Huang).

^{*} Corresponding author.

thiolate chromatography) to remove [8,14]. Some steryl ethers coelute exactly with alkenones on GC-FID, resulting in hard-to-detect, misleading $U_{37}^{K'}$ values [8,15]. Additionally, recent studies have demonstrated major advantages of measuring longer than C_{37} alkenones for sea ice reconstructions in high latitude [16] and SST in tropical warm oceans [17], as well as in saline lakes [18,19]. Simultaneous quantification of alkenones of all chain lengths in sediments, rather than C_{37} only [20], also enhances the fidelity of alkenones as a proxy for paleo-productivity. High-resolution paleo-studies often require analyzing hundreds to thousands of samples [21]. More sensitive and efficient analytical methods can also save time, analytical expenses and increase data reliability.

Ammonia GC-chemical ionization-mass spectrometry (GC-CI-MS) has been successfully applied to analyze alkenones in complex samples [22-24]. It allows selective ion monitoring of alkenones to exclude coeluting compounds and has ~2 times lower limit of detection (LOD) than GC-FID. However, GC-CI-MS faces critical challenges: 1) Substantial non-linear responses [25]: the degree of such non-linearity, even for the same instrument, can fluctuate significantly over time. Ionization efficiency of individual alkenones is highly sensitive to small changes in the ion source, such as temperature, ammonia gas pressure, leading to the need for frequent recalibrations [22]. 2) Large differences in response factors among different alkenones, resulting in a polynomial conversion between GC-FID and GC-CI-MS results [25]. 3) $U_{27}^{K'}$ computed from GC-CI-MS shows considerable drift over different injection masses [22,25]. In addition, such drift is not reproducible for the same instrument and can be as much as 0.08 (or \sim 2.4 $^{\circ}$ C inferred temperature) in opposite directions as the injection mass increases from 30 to 400 ng [22]. To minimize these effects, injection masses must be confined to a narrow range (e.g., 3-30 ng) [22]. 4) Operation and calibration of GC-CI-MS require substantial technical expertise and interrupt the use of GC-MS in electron ionization (EI) mode for biomarker identifications. These problems have prevented GC-CI-MS from becoming a routine analytical tool for alkenones.

This study aims to develop reversed-phase HPLC-MS methods for analyzing alkenones that are easy-to-implement and exhibit high selectivity, linearity and sensitivity. We compare method efficacies (i.e., LODs, linearity, response factors, selectivity) in single quadrupole, Orbitrap, and quadrupole time of flight (qTOF) mass spectrometers, as well as two ionization modes (APCI vs. ESI) relative to GC-FID. We examine alkenones from Isochrysidales cultures, sample that contains double bond positional isomers, core-top sediments from global ocean sites and sediment sample that contains large amounts of coeluting steryl ethers and wax esters. The advantages and limitations of each instrument for practical application in organic geochemistry, paleoceanography and paleoclimatology laboratories are also assessed.

2. Experimental section

2.1. Materials

All solvents were HPLC grade from Fisher Scientific (USA). Ammonium hydroxide solution (14.8 M) was purchased from Fisher Scientific (USA). Formic acid (97.5–98.5%) was purchased from Millipore-Aldrich (USA). Zorbax Eclipse PAH column (2.1 mm \times 100 mm x 3.5 μ m) was purchased from Agilent (USA). ACE UltraCore super C18 column (2.1 mm \times 250 mm x 5 μ m) was purchased from Mac-Mod (USA).

2.2. Culture and sediment samples

Samples analyzed in this work include: 1) 19 samples from different cultured Isochrysidales including *Isochrysis nuda* RCC1207, *Emiliania huxleyi* NIES3366, *Gephyrocapsa oceanica* RCC6484 and RCC3483 and Group 2i RCC5486 (details of culture experiments and alkenone extraction protocols can be found in Liao et al., 2020, 2021, 2022a, b)

[18,26–28]. 2) 42 core-top ocean sediments from different sites globally with a mean annual SST from 0.1 to 29.5 °C. These core-top samples were initially obtained for the establishment of global temperature calibrations of $U_{38\text{Me}}^{K'}$ index using GC-FID [17], where $U_{38Me}^{K^{'}} = C_{38:2Me}/(C_{38:2Me} + C_{38:3Me})$ and $C_{38:2Me}$ and $C_{38:3Me}$ represent C_{38} methyl alkenones with two and three double bonds, respectively. 3) one down-core sediment sample from West Greenland core 343310 collected during the Maria S. Merian expedition MSM05/03 with depth of 5.04 m below sea floor (mbsf), which shows extensive co-elution between alkenones and steryl ethers (as well as other compounds) on GC-FID [8, 29]. 4) one surface sediment from Lake Braya Sø, Greenland that contains alkenone double bond positional isomers. This sample was used as a standard sample to monitor the instrument status and develop HPLC methods, as the desired HPLC method should be capable of resolving the double bond positional isomers [30]. Details of these samples are provided in Table S1. Before HPLC analysis, these samples were analyzed by GC-FID using parameters described in Liao et al., 2020 [18].

2.3. Development of HPLC-MS methods

Extensive experiments to optimize chromatographic separations using different HPLC columns and solvent schemes were performed. Two different HPLC columns (a Zorbax Eclipse PAH column: 2.1 mm \times 100 mm x 3.5 μm and an ACE UltraCore super C18 column: 2.1 mm \times 250 mm x 5 μm) were used for separations (solvent gradients are provided in corresponding figure legends). Because alkenones contain over 37 carbons and are strongly hydrophobic, we performed extensive tests to identify water-free solvent combinations that not only allow baseline separations of critical alkenones with mass overlaps, but also facilitate initial sample dissolution. Different solvents are systematically tested and eventually selected for ESI and APCI modes, which are discussed in detail in Section 3.1.

Four different mass detectors with either ESI or APCI modes were evaluated in this study: ESI-Quadrupole-MS, APCI-Quadrupole-MS, ESI-Orbitrap-MS and ESI-qTOF-MS. Analyses using HPLC-ESI/APCI-Quadrupole-MS were performed on Agilent 1200 series HPLC system coupled to a quadrupole LC/MS detector (Agilent 6130 series) equipped with ESI/APCI source. Analyses using HPLC-ESI-Orbitrap-MS were performed on Thermo Fisher Scientific Q-Exactive Plus Orbitrap Mass Spectrometer equipped with a heated electrospray interface (ESI) coupled to a Vanquish UHPLC. Analyses using HPLC-ESI-qTOF-MS were performed on Agilent 1290 series UPLC system coupled to Agilent 6530 qTOF mass spectrometer with an Agilent jet stream dual electrospray ionization (ESI) interface. Detailed MS parameters for all instruments are summarized in Table S2.

2.4. Development of calibration methods

As mass spectrometers showed varied response factors towards alkenones that differ in chain lengths/double bond positions/terminal groups, direct HPLC-MS measurements generally yield different alkenone unsaturation ratios from those obtained via conventional GC-FID measurements. It is therefore necessary to convert the HPLC-MS measurements to GC-FID compatible results. We systematically compared two different calibration methods in this study: 1) calibration through absolute concentrations of individual alkenones (the conventional approach); and 2) calibration through a set of alkenone standards with a broad range of unsaturation ratios grown in the laboratory cultures. The second approach takes the advantage of the fact that alkenone paleothermometers are based on ratios of alkenones containing different numbers of double bonds, rather than absolute concentrations. It effectively cancels any instrument instabilities and yields superior results. Details for comparing the two calibration approaches are discussed in detail in Section 3.5. Further validation of our newly developed calibration approach is presented in Section 3.6.

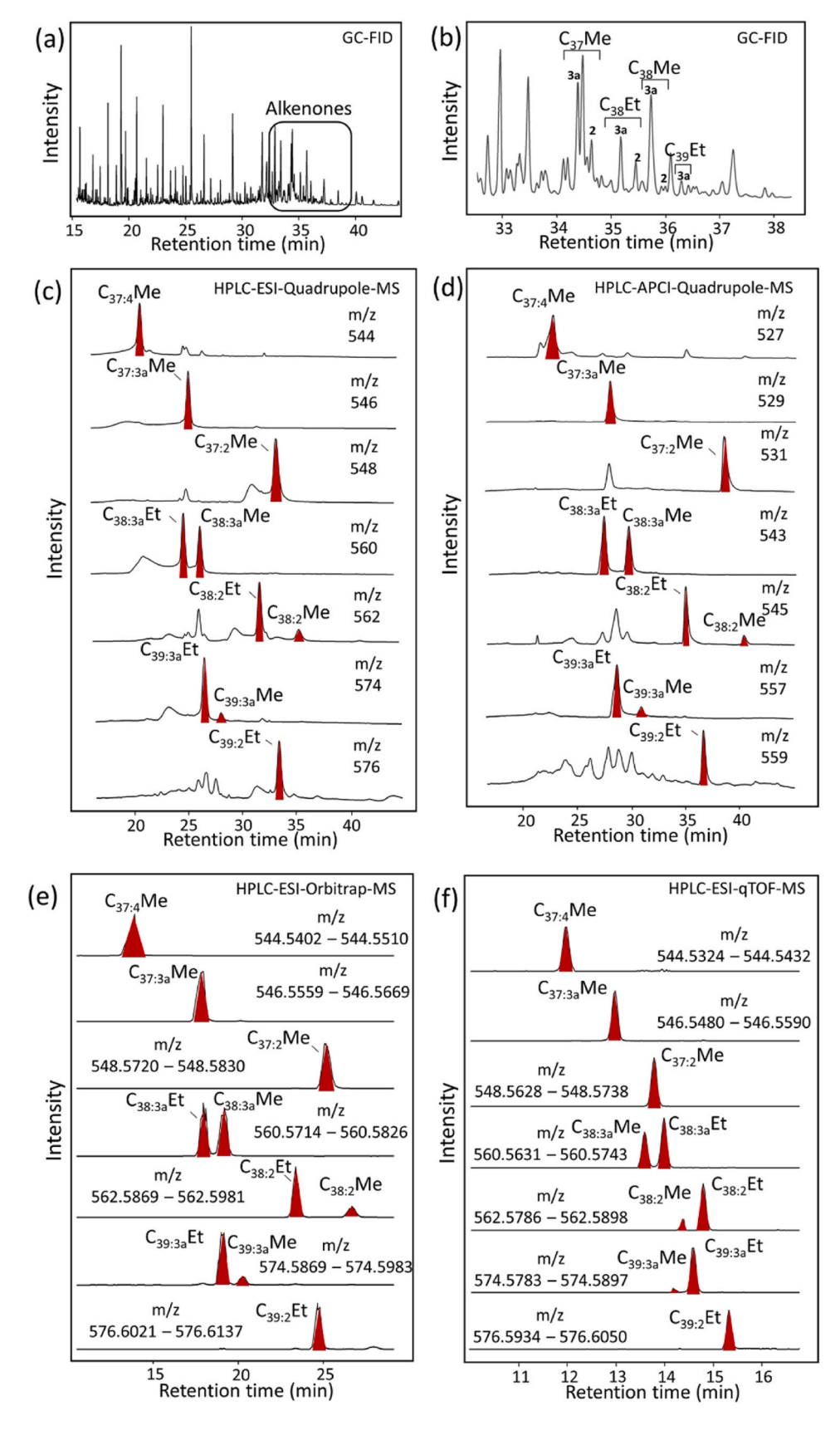


Fig. 1. Chromatograms showing the distribution of alkenones from sediments of West Greenland Core 343310 at 5.04 m below sea floor (mbsf) using (a, b) GC-FID, (c) HPLC-ESI-Quadrupole-MS, (d) HPLC-APCI-Quadrupole-MS with the same HPLC column and mobile phase gradient as used for HPLC-ESI-Quadrupole-MS, but using methanol as solvent A and hexane/2-propanol (v/v 50:50) as solvent B. (e) HPLC-ESI-Orbitrap-MS with the same HPLC column, mobile phase composition and gradient as used for HPLC-ESI-Quadrupole-MS. The mass tolerance window was 10 ppm. (f) HPLC-ESI-qTOF-MS with an ACE UltraCore super C18 column (2.1 mm \times 250 mm x 5 μ m, Aberdeen, UK). The mass tolerance window was 10 ppm. Detailed information of HPLC methods used in each instrument setting could be found in Table S2. In GC-FID chromatograms, numbers above each peak represent the number of C=C bonds in corresponding alkenones. Alkenone masses measured using Orbitrap and qTOF are slightly different possibly related to differences in mass calibrations. Alkenone peaks were highlighted with red color. All LC/MS parameters were summarized in Table S2.

3. Results and discussion

3.1. Chromatographic separation of alkenones

Becker et al. (2015) have previously reported using normal-phase HPLC with APCI source to analyze alkenones [31]. However, the normal-phase column used in the study has poor resolution between alkenones with different number of double bonds (e.g., $C_{37\cdot3}$ and $C_{37\cdot2}$) and of different chain lengths. The poor chromatographic separation of the normal-phase HPLC means that accurate quantification of individual alkenones relies on the resolution of the mass spectrometer and mass overlap from alkenones that would bias the quantification results. For example, using an APCI source, the extracted m/z feature at 531 contains both the isotopologue peak of $C_{37:3}$ ([M + H+2]⁺) and pseudo molecular ion peak of C_{37:2} ([M+H]⁺). In addition, C_{37:4} partially coelutes with $C_{38:2}$ Me. $C_{37:4}$ has the pseudo molecular ion at m/z 527. However, m/z 527 also exists in the APCI mass spectra of $C_{38:2}$ (pseudo molecular ion at m/z 545) due to a loss of water (m/z 545–18 = 527)

We used alkenones, including double bond positional isomers of triunsaturated alkenone, isolated from Lake Braya Sø surface sediment, southwestern Greenland to develop reversed-phase HPLC separation methods [30,32]. After extensive tests using different solvent combinations, baseline resolutions of all critical alkenone pairs were achieved using a Zorbax Eclipse PAH column (Fig. 1; Fig. S3b). For ESI mode, the selected mobile phase was composed of methanol/formic acid/14.8 NH₃ (100:0.04:0.1, solvent A) and hexane (hex)/2-propanol (IPA)/formic acid (FA)/14.8 M NH₃ (50:50:0.04:0.1, solvent B), with solvent gradient specified in Fig. 1. For APCI mode, solvent A is methanol and solvent B is hexane/2-propanol (v/v 50:50) (Fig. 1). Notably, no water in the initial solvents was required to achieve our desired separation of alkenones, which facilitates the initial dissolution of highly hydrophobic alkenones in water-free solvents (Fig. 1). Baseline resolution was achieved between 1) alkenones with different number of double bonds (e.g., C37:3 and C37:2, $R_s = 6.1$), which permits accurate calculation of different alkenone-based proxies such as $\mathrm{U}_{37}^{\mathrm{K}} = (\mathrm{C}_{37:2} - \mathrm{C}_{37:4})/(\mathrm{C}_{37:2} + \mathrm{C}_{37:3} + \mathrm{C}_{37:4})$ and $\mathrm{U}_{37}^{\mathrm{K'}} = \mathrm{C}_{37:2}/\mathrm{C}_{37:4}$ $(C_{37:2} + C_{37:3})$ for paleo-temperature reconstructions [1,2,5,8,33]; 2) double bond positional isomers of tri-unsaturated C_{37} alkenones ($C_{37:3a}$ and $C_{37:3b}$, $R_s = 2.2$, where a and b represent isomers with $\Delta^{7,14,21}$ and $\Delta^{14,21,28}$ double bond positions, respectively) with the same molecular weights [34]. This allows accurate calculation of RIK₃₇ = $C_{37:3a}/(C_{37:3a}+C_{37:3b})$ (ratio of isomeric C₃₇ ketones) proxy that has been used for salinity reconstructions [6.7.32] and 3) C_{38} Me and C_{38} Et alkenones (e.g., $C_{38:2}$ Et and $C_{38:2}$ Me, $R_s =$ 2.7, where Et and Me represent ethyl and methyl ketones, respectively) with the same molecular weights. This approach allows for accurate calculation of $U_{38Me}^{K'} = C_{38:2Me}/(C_{38:2Me} + C_{38:3Me})$ which has been proposed to be a better SST proxy in sites with mixed alkenone production from different groups of Isochrysidales [5,8], as well as in warm oceans [17,35]. Alkenones with same number of double bonds but of different chain lengths share similar retention times and partially co-elute with each other (e.g., co-elution between C37:4 and C38:4Et and between C37:3a and C38:3aEt, Fig. S3b). Fortunately, for both APCI and ESI, there are no mass overlaps for these alkenones (Figs. S1-2). Thus, these alkenones were well-resolved in the extracted ion chromatograms (EICs) (Fig. S3).

We also tested an ACE UltraCore Super C18 column (Fig. 1f), which is believed to have higher packing efficiency and plate number, smaller pore volume and mass transfer resistance than traditional porous columns due to its solid core-shell structure [36,37]. Core-shell HPLC columns also allow for faster analysis of samples than the porous column (17 min vs. 40 min contrast in our case; Figs. S3-4) [38]. A marked difference in elution patterns was observed, with the ACE column showing that: 1) methyl alkenones elute earlier than ethyl alkenones, 2) Tri-unsaturated alkenones with double bonds at $\Delta^{7, 14, 21}$ elute later than alkenones with double bonds at $\Delta^{14, 21, 28}$ (e.g., $C_{37:3a}$ elutes later than C_{37:3b}, C_{38:3a} elutes later than C_{38:3b}), and 3) Primary separation is based

Summary of major differences among instrument suites tested in this study for analyses of alkenones.	nent suites tested in thi	is study for analyses of alkenones.					
Analytical methods	Instrument price	Selectivity towards alkenones ^a	Limit of detection (pg)	Linearity dynamic range tested $(ng)^b$	Response	e factors rela	Response factors relative to ${\sf C}_{37:2}^{\rm c}$
					C _{37:4}	C _{37:3a}	C _{37:3b}
HPLC-ESI-Quadrupole-MS	Medium	Medium	8.6	1.8–54.2	0.92	1.18	1.22
HPLC-APCI-Quadrupole-MS (Reversed-phase)	Medium	Medium	48.0	1.8–54.2	6.26	3.70	3.37
HPLC-ESI-Orbitrap-MS	High	High	0.4	0.0090–5.4	1.53	0.99	1.27
HPLC-ESI-qTOF-MS	High	High	3.8	0.45-9.0	1.76	1.00	1.87
HPLC-APCI-qTOF-MS (Normal-phase) [31]	High	High	$< 10^{ m d}$		\	0.77	\
GC-CI-MS [22,25,41]	Low to Medium	Medium	10	$\sim 5-20^{\circ}$	\	0.62	\
GC-FID [18,25,42]	Low	Low (non-selective)	20		\	1.00	\

^a Capability to resolve alkenones from interfering compounds using ion selective detection.

b Injection amount of C₃₇₋₄ in surface sediment sample from Lake Braya Sø, Greenland. The upper limit of dynamic range is conservatively estimated as further increase in the injection amounts led to partial coelution between C_{38:3b}Et and C_{38:3a}Me which have the same molecular weights.

 $^{^{\}rm d}$ Limit of quantification (instead of limit of detection), as reported in Becker et al. (2015) [31]. Based on slopes of the calibration curves of different alkenones.

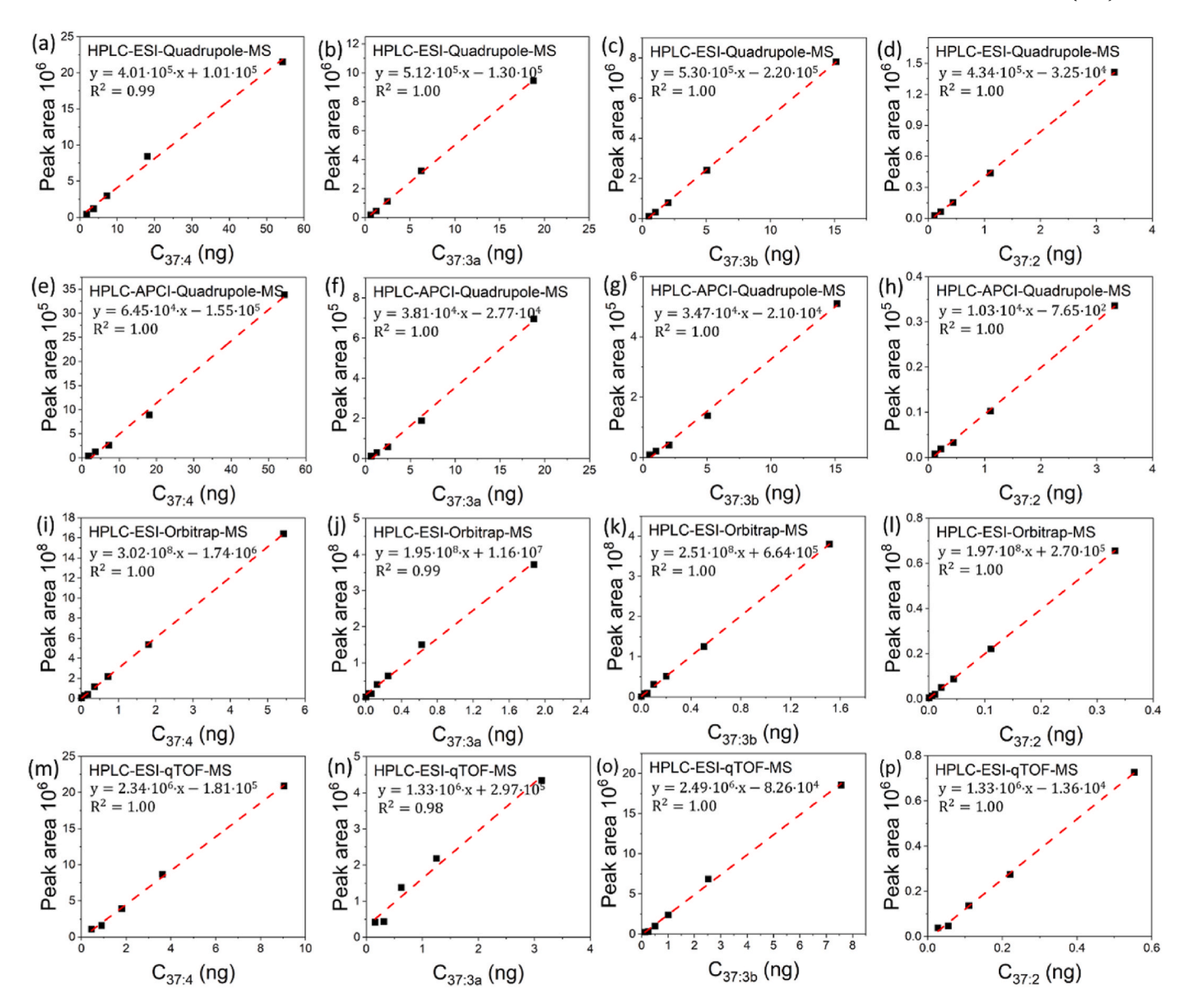


Fig. 2. Response factor calibrations for (a) $C_{37:4}$, (b) $C_{37:3a}$, (c) $C_{37:3b}$ and (d) $C_{37:2}$ using HPLC-ESI-Quadrupole-MS; (e) $C_{37:4}$, (f) $C_{37:3a}$, (g) $C_{37:3b}$ and (h) $C_{37:2}$ using HPLC-ESI-Orbitrap-MS and (m) $C_{37:4}$, (n) $C_{37:3a}$, (o) $C_{37:3b}$ and (p) $C_{37:2}$ using HPLC-ESI-QUADRUPOLE-MS; (i) $C_{37:3b}$ and (j) $C_{37:3b}$ and (l) $C_{37:2}$ using HPLC-ESI-Orbitrap-MS and (m) $C_{37:4}$, (n) $C_{37:3a}$, (o) $C_{37:3b}$ and (p) $C_{37:2}$ using HPLC-ESI-QUADRUPOLE-MS; (e) $C_{37:3b}$ and (f) $C_{37:3b}$ and (g) $C_{37:3b}$ and (g)

on chain length, with shorter-chain alkenones elute earlier (Fig. S4). However, ACE UltraCore Super C18 column did not fully resolve double bond positional isomers (e.g., for $C_{37:3a}$ and $C_{37:3b}$, $R_s = 0.6$, Fig. S4). Although the reasons for these differences are not clear, for samples from ocean and saline lakes that do not contain double bond positional isomers, the core-shell column is likely to perform better than a Zorbax column as it provides faster analysis and excellent resolution for alkenones used for computing paleotemperature proxies in ocean environments.

3.2. Mass selective detection in samples containing large amounts of coeluting compounds

To compare the ability of different mass detectors to resolve alkenones in complex samples, we selected the ocean sediment sample collected off west Greenland, which is well known for containing exceptionally large amounts of steryl ethers and wax-esters that co-elute with alkenones (Fig. 1a-b) [8]. In contrast to the extensive coelution of alkenones in the GC-FID chromatogram (Fig. 1a-b), extracted

pseudo-molecular ion chromatograms of targeting alkenones were much cleaner using HPLC-single quadrupole MS equipped with ESI and APCI sources (Fig. 1c–d). However, probably due to the relatively low resolution of the mass analyzer, EICs from single quadrupole MS may still contain some isotopologue overlaps from unknown components, leading to uneven baselines (Fig. 1c–d).

Use of high-resolution Orbitrap and qTOF mass detectors yielded clean extracted ion chromatograms with flat baselines (Fig. 1e–f). The selection of different mass tolerance windows (e.g., 1 ppm, 10 ppm, 20 ppm, 50 ppm) in the Orbitrap MS did not affect the integration results, with relatively small mass tolerance window (\leq 10 ppm) eliminating all interference. Collectively, our results demonstrate that high resolution HPLC-MS instruments are very effective at eliminating interference from coelution in complex natural sediment samples.

3.3. Sensitivity, linearity and response factors

Method sensitivity, assessed as the limit of detection (defined as three times of signal-to-noise ratio) of the HPLC-MS measurements, was

determined using the surface sediment of Lake Braya Sø. With the single quadrupole MS, ESI provided a lower LOD (8.6 pg injected mass) than APCI (48.0 pg injected mass), most likely due to ESI's higher ionization efficiency towards alkenones. The LOD using ESI-Quadrupole-MS was slightly lower than the value reported for GC-FID (20 pg) and GC-CI-MS

(10 pg) (Table 1). Among the three mass detectors tested in ESI mode, the Orbitrap (0.4 pg) provided the lowest LOD, followed by qTOF (3.8 pg), and in turn by the single quadrupole MS (8.6 pg). Higher mass resolution in Orbitrap and qTOF allows greater selectivity and noise reduction. In addition, ESI sources utilized in our Orbitrap and qTOF

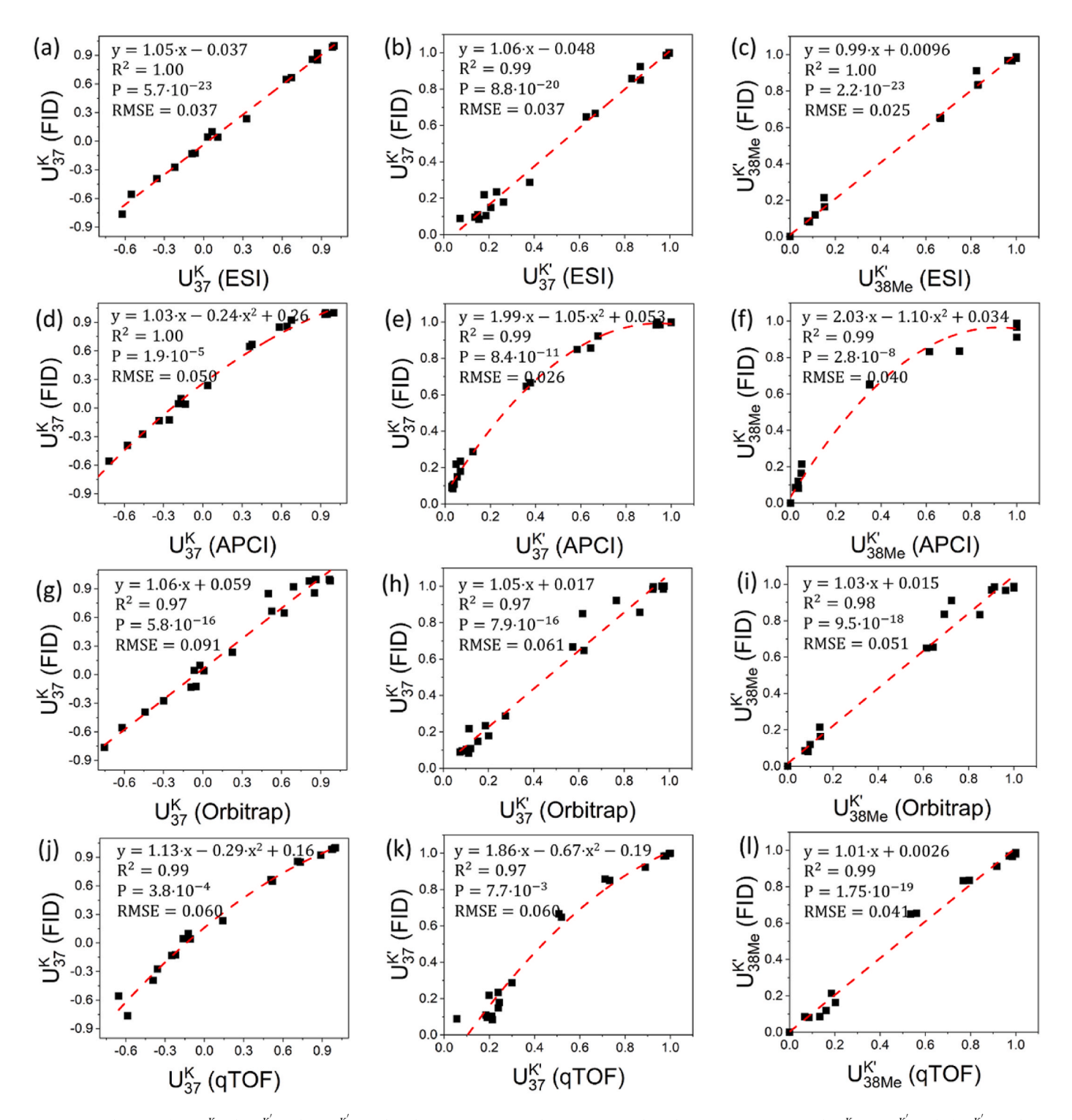


Fig. 3. Correlations of (a) U_{37}^K , (b) $U_{37}^{K'}$ and (c) $U_{38Me}^{K'}$ values between GC-FID and HPLC-ESI-Quadrupole-MS measurements; (d) U_{37}^K , (e) $U_{37}^{K'}$, and (f) $U_{38Me}^{K'}$ values between GC-FID and HPLC-ESI-Quadrupole-MS measurements; (g) U_{37}^K , (h) $U_{37}^{K'}$ and (i) $U_{38Me}^{K'}$ values between GC-FID and HPLC-ESI-Orbitrap-MS measurements; and (j) $U_{37}^{K'}$, (k) $U_{37}^{K'}$, and (l) $U_{38Me}^{K'}$ values between GC-FID and HPLC-ESI-QTOF-MS measurements. Various HPLC-MS derived proxy values were computed directly from EIC peak areas. Analyses were performed on 19 Isochrysidales culture samples grown at different temperatures (including *I. nuda* at 4, 15 and 25 °C, *G. oceanica* RCC3483 and *G. oceanica* RCC6484 at 24, 26, 28, 30, and 32 °C, *E. huxleyi* NIES3366 at 3, 6, 9, 12 and 15 °C as well as *Isochrysis sp.* RCC5486 at 3 °C) and 1 sediment sample from Lake Braya Sø.

instruments have more advanced features (e.g., jet stream dual ESI interface), which may have enhanced ionization efficiency [39].

Highly sensitive detection of alkenones is not only important for sites with low alkenone concentrations, but also for 1) detecting extended chain length alkenones and alkenoates which help disentangle different Isochrysidales production and extract seasonal temperature signals in ocean and saline lakes [7,18] and 2) temperature reconstruction in warm ocean sites (e.g., Pacific Warm Pool) with trace amounts of $C_{37:4}$ and $C_{37:3}$ that are not detected/quantified by GC-FID [40]. Representative EICs obtained using HPLC-ESI-Orbitrap MS to detect extended chain length alkenones and alkenoates in the sample of *I. nuda* cultured at 4 °C and trace amount of tetra- and tri-unsaturated alkenones in the sample of *G. oceanica* cultured at 28 °C are shown in Fig. S5. Notably, $C_{37:4}$ and $C_{37:3}$ cannot be detected in the same *G. oceanica* sample using GC-FID (Fig. S5b).

All HPLC-MS instruments displayed excellent linearity over a relatively wide range of injected masses (Fig. 2). The single quadrupole MS, operated in ESI or APCI mode, showed linear responses of injected mass of alkenones ranging from 1.8 to 54.2 ng (30-fold) with $R^2=1$ (Fig. 2a–h). Further increasing the injected mass led to partial coelution of $C_{38:3b}$ Et and $C_{38:3a}$ Me which share the same molecular weight. By far the instrument that offers the highest linear dynamic range is the Orbitrap MS. In our test, the Orbitrap MS achieved excellent linear response for alkenones with injection amounts ranging from 0.009 to 5.4 ng or 600-fold of dynamic range (Fig. 2i-l). Similarly, within the range of concentration tested (0.45–9 ng, or 20-fold), qTOF also offers excellent linear response (Fig. 2m-p).

Different HPLC-MS instruments operated in ESI mode show different response factors among different alkenones. Single quadrupole MS in ESI mode showed the most similar response factors among alkenones with different numbers of double bonds, chain lengths, terminal methyl/ethyl groups and double bond positions, with $C_{37:4}$, $C_{37:3}$ and $C_{37:2}$ differing by only 10-20% (Table 1). In comparison, single quadrupole MS in APCI mode was more sensitive to alkenones with more double bonds (e.g., response factor of $C_{37:4}$ and $C_{37:3a}$ is 5.26 and 2.7 times greater than that of $C_{37:2}$; Table 1). Notably, however, Becker et al., 2015 observed the opposite difference using normal phase HPLC-MS in APCI mode, with $C_{37:2}$ more responsive than $C_{37:3}$ by 30% [31]. Therefore, response factors are also sensitive to a range of operating conditions, including normal versus reversed-phase HPLC, different instruments and ionization methods.

It is particularly encouraging to observe that the Orbitrap MS, with its exceptional sensitivity and linearity, also displays nearly identical response factors for $C_{37:3a}$ and $C_{37:2}$ (Table 1). This means that $U_{37}^{K'}$ values calculated directly from Orbitrap data would be virtually identical to those obtained from GC-FID measurement. However, we noticed that the response factor of $C_{37:3b}$ is 27% greater than $C_{37:3a}$, and $C_{37:4}$ is 53% greater than $C_{37:2}$ (Table 1). These large differences in response factors indicate that it is necessary to calibrate U_{37}^{K} and RIK₃₇ values obtained from the Orbitrap MS to obtain data compatible with GC-FID results. Similarly, qTOF MS displays identical response factor between $C_{37:3a}$ and $C_{37:2}$ (Table 1). Double bond position effect on response factor is also strong for qTOF, with $C_{37:3b}$ 87% more sensitive to $C_{37:3a}$. $C_{37:4}$ is also 76% more responsive than $C_{37:2}$. These data also suggest that U_{37}^{K} and RIK₃₇ values must be carefully calibrated against GC-FID measurements for qTOF MS.

3.4. Consistency of alkenone proxy values at different injection amounts for the same sample

It is important to demonstrate that over the range of alkenone injection mass, the proxy values obtained are consistent. While alkenone injection amount from a real sample can always be adjusted to the suggested injection range by concentration/dilution of solvents or changing injection volumes, a method that permits a wide range (ratio of

highest injection amounts over the smallest injection amounts) while yielding consistent proxy values is more robust and easier to use. For U_{27}^{K} computed directly from HPLC peak areas, all methods yield relatively consistent values over a concentrating factor of >20 times (Figs. S7a, e, i, m), wider than the range obtained for GC-CI-MS (10 times) [22]. Specifically, the standard deviation (STDEV) of U₃₇ was at 0.025 for ESI and 0.029 for APCI from 3.0 to 91.5 ng with single quadrupole, or at 0.028 for both ESI with high-resolution Orbitrap (0.3-9.1 ng) and qTOF MS (0.8–15.2 ng). It is important to stress that proxy value drift at extremely low injection amounts did NOT originate from non-linearity in measurements. Such drift is inherently due to different calibration equations between the injection amounts and peak areas as shown in Fig. 2 for individual alkenones. This can be readily demonstrated mathematically for U₃₇ (Fig. S8a). We note that a similar phenomenon was previously observed also in GC-CI-MS, but appeared to have been mistakenly interpreted as instrumentally derived analytical errors [22]. For computing U₃₇ values, we suggest following minimal injection amounts to minimize response-factor induced U_{37}^{K} drifts: 0.3 ng for Orbitrap, 0.8 ng for qTOF, 3.0 ng for single quadrupole MS.

 $U_{37}^{K'}$ and $U_{38Me}^{K'}$ values display much smaller drift at low injection mass (Fig. S7). This was anticipated, as these two proxies involve only two alkenones with similar response factors in most cases (Fig. 2). This is very fortunate, as these two proxies are most important for SST reconstructions in the ocean. Due to the similarity in response factors between $C_{37:3a}$ and $C_{37:3b}$, RIK $_{37}$ measured using single quadrupole MS in both ESI and APCI modes showed little drift over the full range of injection mass (1.1–33.9 ng), with STDEV at 0.017 for ESI and 0.0061 for APCI, respectively (Figs. S7d and h). However, due to large differences in response factors for $C_{37:3a}$ and $C_{37:3b}$ (e.g., for Orbitrap, intercept is $1.16\cdot10^7$ for $C_{37:3a}$ but $6.64\cdot10^5$ for $C_{37:3b}$ in Fig. 2), there are much larger drifts at different injection amounts using high-resolution MS (Figs. S7l and p). A similar trend can also be obtained theoretically using response factor calibration lines of $C_{37:3a}$ and $C_{37:3b}$ shown in Fig. 2 (Figs. S8b–c).

3.5. Transformation of HPLC-MS measurements to GC-FID compatible proxy values

There are two different strategies to compute proxy values after an instrument measurement is made: 1) Establish a calibration between HPLC-MS-measured "pseudo" proxy values computed directly from measured peak areas from a series of standards with known proxy values measured using GC-FID. Subsequently, use this calibration to convert the HPLC-MS-measured "pseudo" proxy values from real samples to those compatible with GC-FID measurements. 2) Convert the measured peak areas of relevant compounds to corresponding absolute quantities using the correlation between injection quantities and peak areas preestablished (i.e., external calibration equations, as shown in Fig. 2), and then use the absolute quantities of individual compounds to compute the proxy values.

The first strategy is recommended because all alkenone proxy values are relative ratios among different alkenones. This is analogous to measuring stable isotopic ratios where a series of isotopic standards with known isotopic values are first measured on the instrument. A regression of authentic ratios and the measured ratios of the standards is then established. This regression was subsequently used to convert measured ratios in real samples to values compatible to isotopic standards. This approach effectively eliminates errors in alkenone ratios derived from instrumental drifts over time because a fluctuation in instrument sensitivity would likely affect all compounds equally and proportionally. We note that calibrating the instrument against a series of reference standards encompassing the same or a larger $U^{K'}_{37}$ range as that in the samples of study has been previously suggested for GC-CI-MS measurements as well [41]. We further compare the results of using both

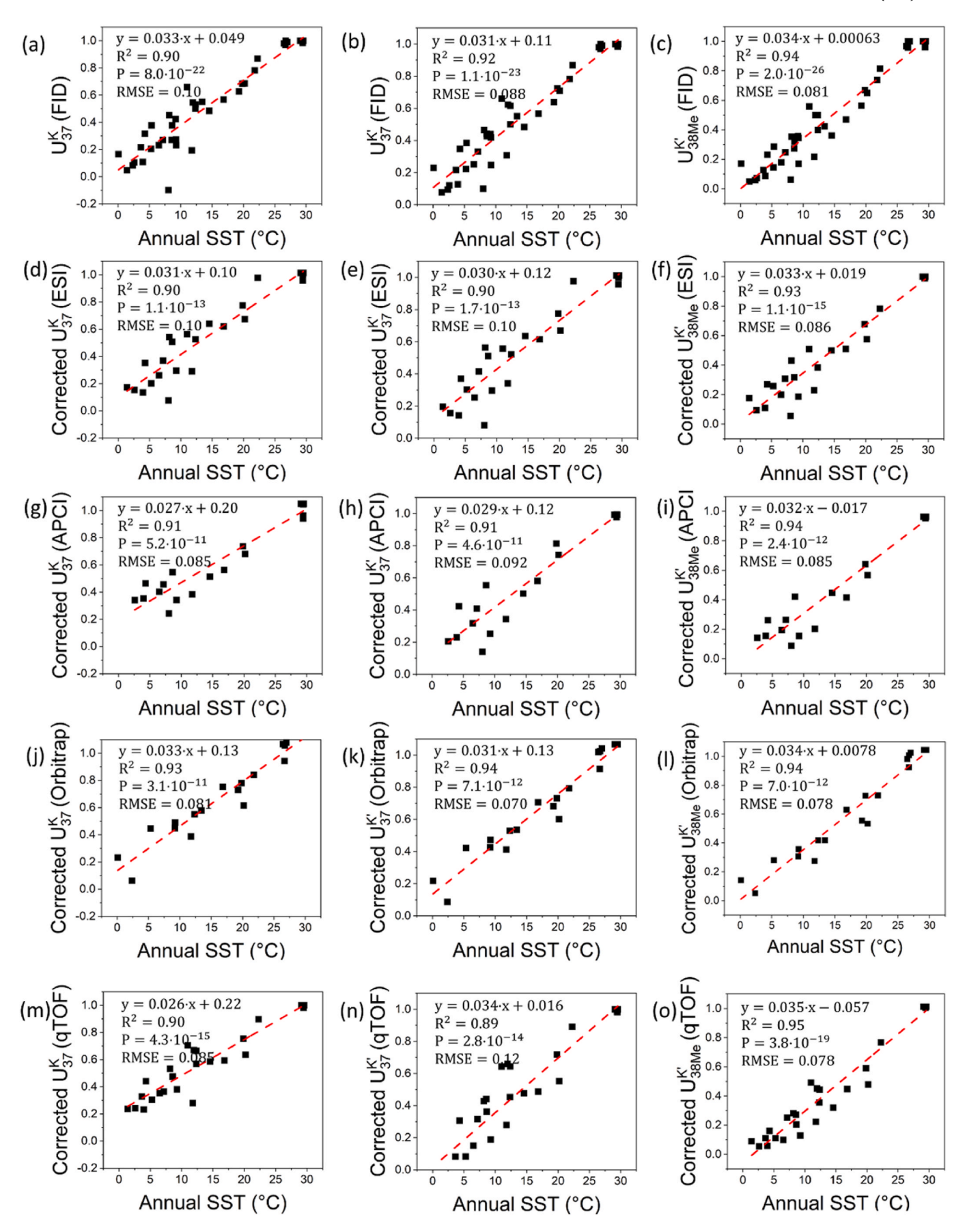


Fig. 4. Calibrations of (a) U_{37}^{K} , (b) $U_{37}^{K'}$ and (c) $U_{38Me}^{K'}$ to annual SST based on global core-top sediments using GC-FID (N = 42). Calibrations of corrected (d) $U_{37}^{K'}$, (e) $U_{37}^{K'}$ and (f) $U_{38Me}^{K'}$ to annual SST using HPLC-ESI-Quadrupole-MS (N = 26). Calibrations of corrected (g) U_{37}^{K} , (h) $U_{37}^{K'}$ and (i) $U_{38Me}^{K'}$ to annual SST using HPLC-APCI-Quadrupole-MS (N = 20). Calibrations of corrected (j) U_{37}^{K} , (k) $U_{37}^{K'}$ and (l) $U_{38Me}^{K'}$ to annual SST using HPLC-ESI-Orbitrap-MS (N = 19). Calibrations of corrected (m) U_{37}^{K} , (n) $U_{37}^{K'}$ and (o) $U_{38Me}^{K'}$ to annual SST using HPLC-ESI-qTOF-MS (N = 29). Corrections of HPLC proxy values were achieved by converting "pseudo" HPLC proxy values (computed directly based on peak areas) to corresponding GC-FID values using the correction equations established in Fig. 3. Number of data points available for individual methods was different due to sample consumption caused by repeated injections. Detailed information for the ocean core-top sediments used are given in Table S1.

strategies to compute the proxy values in a set of surface sediments from global oceans in Section 3.6.

Calibration curves between "pseudo" proxy values of $U^{K}_{37},\,U^{K^{'}}_{37}$ and $U_{38Me}^{K'}$ computed directly from measured HPLC-MS peak areas and authentic proxy values (pre-measured using GC-FID) were established from 20 standard samples selected to cover a wide range of proxy values (Fig. 3). Excellent linear relationships between the "pseudo" proxy values from HPLC-MS and real values from GCF-ID for U_{37}^K , $U_{37}^{K'}$ and $U_{38Me}^{K'}$ were obtained for single quadrupole MS (ESI) and Orbitrap MS (ESI) (Fig. 3a-c, g-i). In both cases, we obtained slopes that were very close to 1 with very small y-axis intercepts, indicating that numeric proxy values measured from HPLC-MS peak areas were in fact very similar to the authentic values measured using GC-FID. The main reason for these strong linear relationships and small intercepts between HPLC-MS measurements and real values was that response factors (or equations between injection amounts and peak areas) for di- and triunsaturated C_{37} and C_{38} alkenones were nearly identical for both single quadrupole (ESI) and Orbitrap (ESI) measurements (Fig. 2b&d, j&l).

However, for single quadrupole MS (APCI) and qTOF (ESI), the relationships between HPLC-MS measurements and real proxy values were best fit using second-order polynomial equations (Fig. 3d-f, j-l). Such non-linear correlations are likely due to the significant differences in response factors for alkenones with different number of double bonds and result in systematic offsets between single quadrupole (APCI), qTOF (ESI) and GC-FID alkenone unsaturation ratio measurements (Fig. 2). Similar non-linear correlations can be obtained theoretically based on the response factor equations for individual alkenones for $U_{37}^{K'}$ from single quadrupole MS (APCI) as shown in Fig. S9. We can also increase the assumed injection mass of C_{37:2} from 10 to 500 ng, and compute corresponding $C_{37;3}$ at the $U_{37}^{K'}$ proxy values ranging from 0.1 to 0.95 at an interval of 0.05. The correlation between calculated HPLC values and corresponding assumed $U_{37}^{K^{\prime}}$ values do not change significantly as the injection mass increases (details in Fig. S9). This analysis suggests that the influence of alkenone injection mass on the calibration curves is small.

3.6. Core-top calibrations of $U_{37}^{\rm K}$, $U_{37}^{\rm K'}$ and $U_{38\rm Me}^{\rm K'}$ to SST: method validation

To validate the calibrations presented in section 3.5, a set of 42 coretop samples was analyzed to compare GC-FID and HPLC-MS-based temperature calibrations (Fig. 4). These samples (Table S1) were first analyzed by GC-FID (Fig. 4a–c). In some cases, the number of samples analyzed by HPLC-MS was fewer than 42, due to excess sample consumption upon repeated injections and/or low alkenone concentrations in the original samples (Fig. 4d-o).

Single quadrupole MS and Orbitrap MS, both in ESI mode, provided excellent linear regressions of all three proxies U_{37}^K , $U_{37}^{K'}$ and $U_{38Me}^{K'}$ against SSTs that are very similar in slopes and intercepts to those obtained from GC-FID (Fig. 4a–f, j-l). Remarkably, corrections using relationships established from standards shown in Fig. 3 made little difference in proxy-SST correlations for both single quadrupole MS and Orbitrap MS as the differences between corrected and uncorrected proxy values were very small (Figs. S11a–c, g-i). This finding is not surprising

because the slopes were close to 1 and intercepts were small between the "pseudo" proxy values and FID results as shown in Fig. 3a–c for single quadrupole MS and Fig. 3g–i for Orbitrap MS, respectively. Interestingly, $U_{37}^{K'}$ to SST correlations were virtually identical using GC-FID, single quadrupole MS (ESI) and Orbitrap (ESI) (Fig. 4b,e,k). These findings indicate that single quadrupole MS and Orbitrap MS in ESI mode are ideal for real world applications, with directly measured values needing virtually no corrections to yield values that are comparable to GC-FID results.

Due to the non-linear relationships between GC-FID results and HPLC-MS measurements (Fig. 3d–f, j-l) originated from relatively large differences in response factors among different alkenones (Fig. 2e–h and m-p), both single quadrupole MS (APCI mode) and qTOF (ESI) yielded greater deviations from GC-FID (Fig. 4g–i, m-o). This was especially true for $\rm U_{37}^{K}$ -SST relationships (Fig. 4g, m), both HPLC-MS settings yield significantly lower slopes (0.027 and 0.026 respectively) than 0.033 from GC-FID measurements. Differences in intercepts to GC-FID were also relatively large for these two HPLC-MS settings. Analytical errors may have been enlarged by the flattening in the higher proxy range in the correction equations (Fig. 3d–f, j-l).

We also tested the second strategy to obtain proxy values (as discussed in beginning of Section 3.5), by first converting the peak areas from HPLC-MS measurements to absolute injection masses, followed by computing proxy values (Fig. S12). As anticipated, in almost all cases, proxy-SST relationships display greater scattering, and correlations display greater dissimilarity to GC-FID results (Fig. 4a–c). This can be explained by instrumental drifts that are difficult to predict when samples are measured at different times, even though we carried out our analyses within 2–3 days after calibration runs. As shown in Fig. S13, computing proxy values from the same sample over different injection amounts using this approach also led to greater fluctuations in proxy values, and drifts in proxy values at low injection amounts are especially large. Using this "external calibration" approach to measure proxy values in real sediment samples would require frequent calibration of instrument responses to a known quantity of alkenones.

4. Conclusions

We developed a reversed-phase HPLC method that permits baseline resolution of alkenones with mass overlaps, including the double bond positional isomers and methyl/ethyl alkenones of the same carbon number with the same molecular weights. Comparison of ESI and APCI on single quadrupole MS suggests that ESI is the more suitable ionization method for alkenone analysis. ESI provides \sim 6 times lower LOD than APCI. Importantly, ESI is much less discriminative among alkenones containing different numbers of double bonds, which results in very similar response factors (or equations) for C_{37:4}, C_{37:3a}, C_{37:3b} and C_{37:2} alkenones in ESI mode. Thus, ESI is preferred over APCI for alkenone analysis.

Among the three mass detectors used, the high-resolution Orbitrap MS offers the lowest LOD (0.4 pg) and widest linear dynamic range (0.0090–5.4 ng). While single quadrupole MS is less sensitive and has narrower linear dynamic range than the Orbitrap MS, its substantially lower cost and much wider availability in organic geochemistry labs make it an excellent tool for the routine analyses of alkenones. It is also the least discriminative in terms of response factors for alkenones

containing different numbers of double bonds. However, for samples whose individual alkenone concentrations are exceedingly low (e.g., <1 ng/g), and/or large amounts of coeluting compounds are present, the Orbitrap MS is a better choice. RP-HPLC-MS in ESI mode should also allow highly sensitive analyses of various aliphatic ketones in complex matrices, especially when an orbitrap MS is used.

We demonstrate converting HPLC-MS measurements of alkenone unsaturation ratios to GC-FID compatible results is best achieved by taking two steps: 1) establish a calibration between HPLC-MS-measured "pseudo" proxy values and "real" values measured using GC-FID by measuring a series of laboratory standards spanning a wide range of proxy values; and 2) use this calibration to convert the HPLC-MS-measured "pseudo" proxy values from real samples to those compatible with GC-FID measurements.

Credit author statement

Sian Liao: Conceptualization, Methodology, Investigation, Writing – original draft Xiao-Lei Liu: Investigation Katherine E. Manz: Investigation Kurt D. Pennell: Investigation, Resources Joseph Novak: Resources Ewerton Santos: Investigation, Yongsong Huang: Writing – review & editing, Supervision, Conceptualization.

Declaration of competing interest

The authors declare that they have no known competing financial interests or personal relationships that could have appeared to influence the work reported in this paper.

Data availability

All data hahve been provided

Acknowledgments

This research was supported by the US NSF grants 1762431 and 2234875 to Y.H., ACS PRF grant 61018-DNI2 to X.-L.L., and the NIEHS Training in Environmental Pathology T32 program (grant #T32ES007272) to K.M. The Thermo LC-Orbitrap MS was partially funded by NSF Major Research Instrumentation (MRI) award CBET-1919870. We thank Woods Hole Oceanographic Institution, Lamont-Doherty Earth Observatory, Oregon State University for providing core-top sediments used for this study. We are also grateful for the comments from the anonymous reviewer.

Appendix A. Supplementary data

Supplementary data to this article can be found online at $\frac{\text{https:}}{\text{doi.}}$ org/10.1016/j.talanta.2023.124653.

References

- [1] S.C. Brassell, G. Eglinton, I.T. Marlowe, U. Pflaumann, M. Sarnthein, Molecular stratigraphy - a new tool for climatic assessment, Nature 320 (1986) 129–133, https://doi.org/10.1038/320129a0.
- [2] P.J. Müller, G. Kirst, G. Ruhland, I. von Storch, A. Rosell-Melé, Calibration of the alkenone paleotemperature index U⁸⁷₅₇ based on core-tops from the eastern South Atlantic and the global ocean (60 degrees N-60 degrees S), Geochem. Cosmochim. Acta 62 (1998) 1757–1772, https://doi.org/10.1016/S0016-7037(98)00097-0.
- [3] J.K. Volkman, G. Eglinton, E.D.S. Corner, T.E.V. Forsberg, Long-chain alkenes and alkenones in the marine coccolithophorid *Emiliania huxleyi*, Phytochemistry 19 (1980) 2619–2622, https://doi.org/10.1016/S0031-9422(00)83930-8.
- [4] T. Herbert, J. Schuffert, D. Thomas, C. Lange, A. Weinheimer, A. Peleo Alampay, J. C. Herguera, Depth and seasonality of alkenone production along the California margin inferred from a core top transect, Paleoceanography 13 (1998) 263–271, https://doi.org/10.1029/98PA00069.
- [5] Y.S. Zheng, P. Heng, M.H. Conte, R.S. Vachula, Y.S. Huang, Systematic chemotaxonomic profiling and novel paleotemperature indices based on alkenones and alkenoates: potential for disentangling mixed species input, Org. Geochem. 128 (2019) 26–41, https://doi.org/10.1016/j.orggeochem.2018.12.008.

- [6] Y. Yao, J. Lan, J. Zhao, R.S. Vachula, H. Xu, Y. Cai, H. Cheng, Y. Huang, Abrupt freshening since the early Little Ice Age in Lake Sayram of arid central Asia inferred from an alkenone isomer proxy, Geophys. Res. Lett. 47 (2020), e2020GL089257, https://doi.org/10.1029/2020GL089257.
- [7] S. Liao, K.J. Wang, Y. Huang, Extended chain length alkenoates differentiate three Isochrysidales groups, Org. Geochem. (2021), 104303, https://doi.org/10.1016/j. orgeochem. 2021.104303
- [8] L. Wang, W.M. Longo, J.T. Dillon, J. Zhao, Y. Zheng, M. Moros, Y. Huang, An efficient approach to eliminate steryl ethers and miscellaneous esters/ketones for gas chromatographic analysis of alkenones and alkenoates, J. Chromatogr. A 1596 (2019) 175–182, https://doi.org/10.1016/j.chroma.2019.02.064.
- [9] M.H. Conte, G. Eglinton, L.A. Madureira, Long-chain alkenones and alkyl alkenoates as palaeotemperature indicators: their production, flux and early sedimentary diagenesis in the Eastern North Atlantic, Org. Geochem. 19 (1992) 287–298, https://doi.org/10.1016/0146-6380(92)90044-X.
- [10] M.W. de Bar, E.C. Hopmans, M. Verweij, D.J. Dorhout, J.S.S. Damsté, S. Schouten, Development and comparison of chromatographic methods for the analysis of long chain diols and alkenones in biological materials and sediment, J. Chromatogr. A 1521 (2017) 150–160, https://doi.org/10.1016/j.chroma.2017.09.037.
- [11] J. Hefter, Analysis of alkenone unsaturation indices with fast gas chromatography/ time-of-flight mass spectrometry, Anal. Chem. 80 (2008) 2161–2170, https://doi. org/10.1021/ac702194m.
- [12] J. Villanueva, J.O. Grimalt, Gas chromatographic tuning of the U^K₃₇ paleothermometer, Anal. Chem. 69 (1997) 3329–3332, https://doi.org/10.1021/ 2007.00382
- [13] A. Rosell Melé, E. Bard, K.C. Emeis, J. Grimalt, P. Müller, R. Schneider, I. Bouloubassi, B. Epstein, K. Fahl, A. Fluegge, Precision of the current methods to measure the alkenone proxy U^K₃₇ and absolute alkenone abundance in sediments: results of an interlaboratory comparison study, G-cubed 2 (2001), https://doi.org/ 10.1029/2000GC000141.
- [14] D.B. Nelson, J.P. Sachs, Concurrent purification of sterols, triterpenols and alkenones from sediments for hydrogen isotope analysis using high performance liquid chromatography, Org. Geochem. 64 (2013) 19–28, https://doi.org/ 10.1016/j.orggeochem.2013.09.005.
- [15] O. Rama-Corredor, A. Cortina, B. Martrat, J.F. Lopez, J.O. Grimalt, Removal of bias in C₃₇ alkenone-based sea surface temperature measurements by high-performance liquid chromatography fractionation, J. Chromatogr. A 1567 (2018) 90–98, https://doi.org/10.1016/j.chroma.2018.07.004.
- [16] K.J. Wang, Y. Huang, M. Majaneva, S.T. Belt, S. Liao, J. Novak, T.R. Kartzinel, T. D. Herbert, N. Richter, P. Cabedo-Sanz, Group 2i Isochrysidales produce characteristic alkenones reflecting sea ice distribution, Nat. Commun. 12 (2021) 1–10, https://doi.org/10.1038/s41467-020-20187-z.
- [17] J. Novak, S.M. McGrath, K.J. Wang, S. Liao, S.C. Clemens, W. Kuhnt, Y. Huang, U^K_{38Me} Expands the linear dynamic range of the alkenone sea surface temperature proxy, Geochem. Cosmochim. Acta (2022), https://doi.org/10.1016/j.
- [18] S. Liao, Y. Yao, L. Wang, K.J. Wang, L. Amaral-Zettler, W.M. Longo, Y. Huang, C₄₁ methyl and C₄₂ ethyl alkenones are biomarkers for Group II Isochrysidales, Org. Geochem. 147 (2020), 104081, https://doi.org/10.1016/j.orgeochem.2020.104081.
- [19] Y. Yao, J. Zhao, R.S. Vachula, S. Liao, G. Li, E.J. Pearson, Y. Huang, Phylogeny, alkenone profiles and ecology of Isochrysidales subclades in saline lakes: implications for paleosalinity and paleotemperature reconstructions, Geochem. Cosmochim. Acta 317 (2022) 472–487, https://doi.org/10.1016/j.gca.2021.11.001.
- [20] M. Raja, A. Rosell-Melé, Appraisal of sedimentary alkenones for the quantitative reconstruction of phytoplankton biomass, Proc. Natl. Acad. Sci. USA 118 (2021), e2014787118, https://doi.org/10.1073/pnas.2014787118.
- [21] T.D. Herbert, L.C. Peterson, K.T. Lawrence, Z. Liu, Tropical ocean temperatures over the past 3.5 million years, Science 328 (2010) 1530–1534, https://doi.org/ 10.1126/science.1185435.
- [22] A. Rosell-Melé, J.F. Carter, A.T. Parry, G. Eglinton, Determination of the $\rm U_{37}^{K'}$ index in geological samples, Anal. Chem. 67 (1995) 1283–1289, https://doi.org/ 10.1021/ac00103a021.
- [23] J. Bendle, A. Rosell-Melé, Distributions of $U_{37}^{K'}$ and $U_{37}^{K'}$ in the surface waters and sediments of the Nordic Seas: implications for paleoceanography, G-cubed 5 (2004) 19, https://doi.org/10.1029/2004GC000741.
- [24] G.H. Haug, A. Ganopolski, D.M. Sigman, A. Rosell-Melé, G.E.A. Swann, R. Tiedemann, S.L. Jaccard, J. Bollmann, M.A. Maslin, M.J. Leng, G. Eglinton, North Pacific seasonality and the glaciation of North America 2.7 million years ago, Nature 433 (2005) 821–825, https://doi.org/10.1038/nature03332.
- [25] R. Chaler, J. Villanueva, J.O. Grimalt, Non-linear effects in the determination of paleotemperature U^c₃₇ alkenone ratios by chemical ionization mass spectrometry, J. Chromatogr. A 1012 (2003) 87–93, https://doi.org/10.1016/S0021-9673(03) 01188-9.
- [26] K.J.W. Sian Liao, Yongsong Huang, Extended chain length alkenoates differentiate three Isochrysidales groups, Org. Geochem. 161 (2021), 104303, https://doi.org/ 10.1016/j.orggeochem.2021.104303.
- [27] S. Liao, Y. Huang, Group 2i Isochrysidales flourishes at exceedingly low growth temperatures (0 to 6° C), Org. Geochem. 174 (2022), 104512, https://doi.org/ 10.1016/j.orggeochem.2022.104512.
- [28] S. Liao, K.J. Wang, Y. Huang, Unusually high production of C_{37:4} alkenone by an Arctic Gephyrocapsa huxleyi strain grown under nutrient-replete conditions, Org. Geochem. (2022), 104539, https://doi.org/10.1016/j.orggeochem.2022.104539.
- [29] M. Moros, J.M. Lloyd, K. Perner, D. Krawczyk, T. Blanz, A. de Vernal, M.-M. Ouellet-Bernier, A. Kuijpers, A.E. Jennings, A. Witkowski, R. Schneider,

- E. Jansen, Surface and sub-surface multi-proxy reconstruction of middle to late Holocene palaeoceanographic changes in Disko Bugt, West Greenland, Quat. Sci. Rev. 132 (2016) 146–160, https://doi.org/10.1016/j.quascirev.2015.11.017.
- [30] W.J. D'Andrea, Y. Huang, Long chain alkenones in Greenland lake sediments: low δ¹³C values and exceptional abundance, Org. Geochem. 36 (2005) 1234–1241, https://doi.org/10.1016/j.orggeochem.2005.05.001.
- [31] K.W. Becker, J.S. Lipp, G.J. Versteegh, L. Wörmer, K.-U. Hinrichs, Rapid and simultaneous analysis of three molecular sea surface temperature proxies and application to sediments from the Sea of Marmara, Org. Geochem. 85 (2015) 42–53, https://doi.org/10.1016/j.orggeochem.2015.04.008.
- [32] J.T. Dillon, W.M. Longo, Y. Zhang, R. Torozo, Y. Huang, Identification of double-bond positions in isomeric alkenones from a lacustrine haptophyte, Rapid Commun. Mass Spectrom. 30 (2016) 112–118, https://doi.org/10.1002/rcm.7414.
- [33] F.G. Prahl, S.G. Wakeham, Calibration of unsaturation patterns in long-chain ketone compositions for paleotemperature assessment, Nature 330 (1987) 367–369, https://doi.org/10.1038/330367a0.
- [34] W.M. Longo, J.T. Dillon, R. Tarozo, J.M. Salacup, Y. Huang, Unprecedented separation of long chain alkenones from gas chromatography with a poly (trifluoropropylmethylsiloxane) stationary phase, Org. Geochem. 65 (2013) 94–102, https://doi.org/10.1016/j.orggeochem.2013.10.011.
- [35] S. Liao, J. Novak, Y. Huang, Exploring the theoretical upper temperature limit of alkenone unsaturation indices: implications for paleotemperature reconstructions, Org. Geochem. 180 (2023), 104606, https://doi.org/10.1016/j. orgeochem.2023.104606.

- [36] F. Gritti, A. Cavazzini, N. Marchetti, G. Guiochon, Comparison between the efficiencies of columns packed with fully and partially porous C₁₈-bonded silica materials, J. Chromatogr. A 1157 (2007) 289–303, https://doi.org/10.1016/j. chroma 2007 05 030
- [37] R. Hayes, A. Ahmed, T. Edge, H. Zhang, Core-shell particles: preparation, fundamentals and applications in high performance liquid chromatography, J. Chromatogr. A 1357 (2014) 36–52, https://doi.org/10.1016/j. chroma.2014.05.010.
- [38] H.A. Naeem, H.D. Sapirstein, Ultra-fast separation of wheat glutenin subunits by reversed-phase HPLC using a superficially porous silica-based column, J. Cereal. Sci. 46 (2007) 157–168, https://doi.org/10.1016/j.jcs.2007.01.002.
- [39] A. Mordehai, J. Fjeldsted, Agilent Jet Stream Thermal Gradient Focusing Technology, Agilent Technologies, Santa Clara, CA, 2009. Technical Note publication No. 5990-3494.
- [40] Y.G. Zhang, M. Pagani, Z. Liu, A 12-million-year temperature history of the tropical Pacific Ocean, Science 344 (2014) 84–87, https://doi.org/10.1126/ science 1246172
- [41] R. Chaler, J.O. Grimalt, C. Pelejero, E. Calvo, Sensitivity effects in U^K₃₇ paleotemperature estimation by chemical ionization mass spectrometry, Anal. Chem. 72 (2000) 5892–5897, https://doi.org/10.1021/ac001014q.
- [42] J.O. Grimalt, E. Calvo, C. Pelejero, Sea surface paleotemperature errors in U^K₃₇ estimation due to alkenone measurements near the limit of detection, Paleoceanography 16 (2001) 226–232, https://doi.org/10.1029/1999PA000440.